

Deposition of mass-selected clusters studied by thermal energy atom scattering and low-temperature scanning tunneling microscopy: An experimental setup

Harald Jödicke, Renald Schaub, Ashok Bhowmick, René Monot, Jean Buttet, and Wolfgang Harbich^{a)}

Institut de Physique Expérimentale, Ecole Polytechnique Fédérale, PHB-Ecublens, CH-1015 Lausanne, Switzerland

(Received 23 December 1999; accepted for publication 7 March 2000)

We present an experimental setup for the investigation of the processes occurring during the deposition of mass-selected clusters on a well-defined surface. The sample is analyzed *in situ* by two complementary methods: thermal energy atom scattering (TEAS) and scanning tunneling microscopy (STM). TEAS is used to study the dynamical processes during the deposition and to gather statistical information about the resulting structures on the surface. Subsequent STM measurements allow us to investigate the collision outcome on an atomic scale. The setup is highly versatile and guarantees ultra-high-vacuum conditions and cryogenic temperatures (≈ 30 K) of the sample at all times even during sample transfer. Clusters are produced in a CORDIS-type cluster source. A new compact multichannel effusive He source in combination with a new Wien-filter-based He detector are used for TEAS measurements. The new low-temperature STM allows measurements in a temperature range between 8 and 450 K. Atomic resolution on the Pt(111) surface is regularly observed at $T_{\text{sample}}=8$ K. The performances of the setup are illustrated by STM images obtained after the deposition of Ag_7^+ clusters with $E_{\text{kin}}=95$ and 1000 eV on bare Pt(111) and by measurements made of the deposition of Ag_7^+ clusters with $E_{\text{kin}}=20$ eV in a Xe-rare-gas matrix adsorbed on Pt(111). © 2000 American Institute of Physics. [S0034-6748(00)00207-0]

I. INTRODUCTION

The fate of mass-selected clusters deposited on a well-defined surface or in a rare-gas matrix depends on a great number of parameters. In recent years, molecular dynamic simulations have been performed to gain microscopic insight into the deposition process in rare-gas matrices and on solid surfaces.¹⁻⁶ Experimental results concerning the collision process between a cluster and a well-defined surface are, however, still sparse. Except for the thermal energy atom scattering (TEAS) results of our group,⁷⁻⁹ almost all results were obtained using either mass spectroscopy of the back-scattered cluster fragments,¹⁰⁻¹³ photoemission,¹⁴⁻¹⁶ Fourier transform infrared,¹⁷ or microscopic methods such as field-ion microscopy,¹⁸ scanning tunneling microscopy (STM),^{19,20} scanning tunneling spectroscopy (STS),²¹ transmission electron microscopy,²² or scanning electron microscopy.²³

The use of rare-gas matrices adsorbed on a surface is a very elegant method to minimize the fragmentation of the clusters and to achieve controlled soft-landing conditions. The low-binding energy between the atoms of the rare-gas matrix allows the cluster to be stopped very softly compared to the abrupt impact on a hard-metal surface.

For small clusters with low-impact energy (<5 eV per

atom), the experiments of Harbich and co-workers^{24,25} have shown that less than 20% of the deposited clusters are fragmented when deposited in matrices of Ar, Kr, or Xe. This is confirmed by molecular dynamics (MD) simulations for $(\text{NaCl})_{32}$,²⁶ Cu_{147} ,² and Cu_2 clusters.²⁷

Ag_7^+ clusters, which have been soft landed on Pt(111) by deposition at 20 eV impact energy on an Ar matrix, and subsequent evaporation of the matrix, have been investigated by STM.²⁸ This study indicates that the damage creation on the surface can be strongly reduced with respect to the case where the same clusters with the same impact energy land on the bare surface.

The wealth of phenomena occurring during and after the deposition can hardly be characterized by a single experimental method. For this reason, we have combined TEAS and STM as the main analytic tools in a new experimental setup, which is presented in this work. The two methods form an ideal combination for the investigation of cluster deposition, or more generally, for the study of disordered surfaces. TEAS allows one to study the dynamical processes occurring on the surface and to gather statistical information about the structures on a macroscopic part of the surface in real time during and after the end of the deposition. The method is nondestructive, allowing us to investigate the same deposit by other methods like STM. The subsequent study of the resulting structures by STM yields complementary information on an atomic scale of the structures on the surface,

^{a)}Electronic mail: wolfgang.harbich@epfl.ch

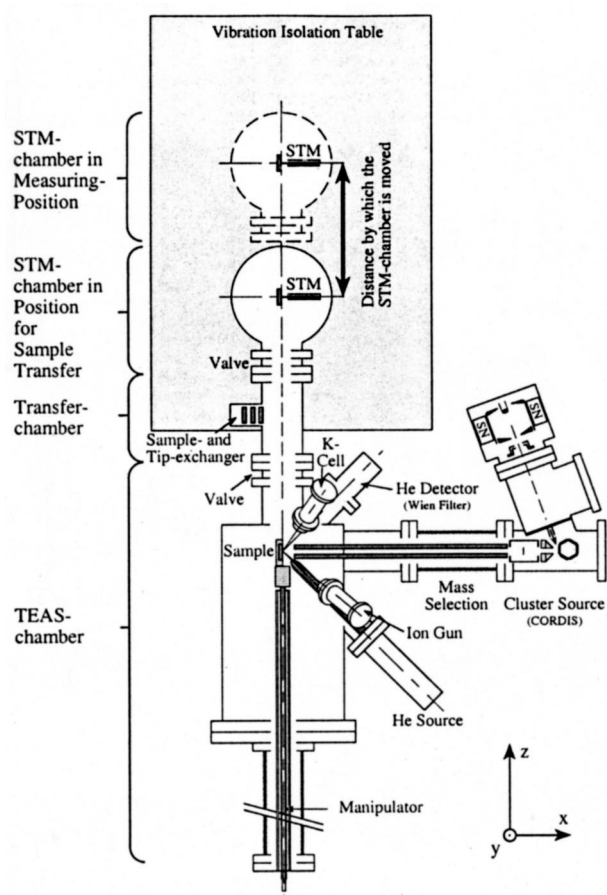


FIG. 1. Layout of the experimental setup with TEAS, STM, and transfer chambers. Two valves allow us to separate the chambers without breaking the vacuum in either of the two main chambers.

which completes the information gathered by TEAS and helps to interpret the TEAS data.

II. EXPERIMENTAL SETUP

A. General overview

The nature of the studied systems and of the chosen analysis methods impose a number of conditions for the experimental setup, which greatly influence its layout. First, UHV conditions are necessary to protect the deposited clusters and the sample surface from contamination from the surrounding atmosphere. Second, to be able to investigate the clusters “as they have been deposited,” it is necessary to freeze thermally activated movements of the cluster and the surface atoms on the surface. For the systems of metal clusters deposited on metal surfaces under consideration, cryogenic temperatures are necessary during the whole duration of the experiment. Finally the microscope must be protected from vibrations produced by the pumps of the TEAS experiment. For this reason, our setup is separated into two chambers, one containing the STM, the other the rest of the experimental equipment. The two chambers are coupled for the TEAS measurements and the sample transfer and mechanically decoupled before the STM measurements.

The layout of the experimental setup is shown in Fig. 1. The TEAS chamber contains the equipment for the sample

preparation, the TEAS measurements, and for the deposition of clusters and atoms from the vapor phase. It is pumped by a 1000 l/s turbomolecular pump, which is backed by another 50 l/s turbomolecular pump to improve He compression. Additional pumping is provided by a titanium-sublimation pump and two cryogenic pumps with a pumping speed of 40 000 l/s. A base pressure $< 1 \times 10^{-11}$ mbar is reached during measurements.

The second chamber of the setup, the STM chamber, is represented once in the sample transfer position (solid lines) and once in the position it is in for the STM measurements (broken lines). The STM chamber holds the STM and its cooling system. During sample transfer and TEAS measurements, the STM chamber is coupled to the TEAS chamber via an intermediate transfer chamber. This allows transferring the sample under UHV conditions and at cryogenic temperatures. The transfer chamber also holds a simple system, based on a linear manipulator, which can stock up to three sample crystals with their sample holders and up to five tips for the STM. Changing of samples and tips is done with the manipulator of the TEAS chamber.

To allow the mechanical separation of the STM chamber from the rest of the experiment, the STM chamber is placed on a rail system. For the STM measurements, the STM chamber is shifted to the middle of a 1600 kg concrete table that is supported by a Newport I-2000 laminar air-flow vibration damping system.²⁹ This system isolates the STM chamber effectively from environmental vibrations. In addition, a completely closed sound-isolating box is placed over the STM chamber to isolate it against acoustic vibrations. Aluminum sheets covering the outer surface of this box act as a Faraday cage. During the STM measurements, the STM chamber is pumped by a vibration-free ion pump (1500 l/s). Additional pumping is obtained by a Titan sublimation pump and by cryogenic pumping. The pressure during the STM measurements is in the order of 1.5×10^{-10} mbar. This value is, however, measured outside the cryostats. We estimate that the pressure inside the cryostats is below this value, as almost all residual gas that enters the cryostat will immediately stick on its cold surfaces. In fact, when the microscope is cooled with liquid helium (LHe), measurements without noticeable pollution are possible for several days after sample preparation.

The transfer of the sample from the TEAS chamber into the STM typically takes 15 min. Another 30 min are necessary to separate the two chambers and to prepare the STM for measurements. Thus, normally first STM images are obtained 45 min after the deposition of the clusters and the end of the TEAS measurements.

The modular layout of the experiment with the STM chamber completely isolated from the rest makes our setup very versatile. First, any additional experimental equipment can be added to the TEAS chamber, without disturbing the STM and second, the transfer chamber allows us, in a simple way, to transfer samples and tips into the two experimental chambers, without breaking the vacuum in either of them.

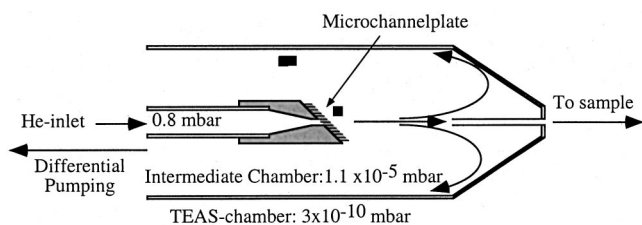


FIG. 2. Schematic representation of the He source. The microchannel plate is glued to the front end of the central tube, which is inclined to account for the channels which are not perpendicular to the surface of the channel plate.

B. TEAS chamber

In this section, the equipment located in the TEAS chamber, namely, the He source, the He detector, the cluster source, and the low-temperature (LT) manipulator, is discussed.

1. He source

To produce the He beam needed for the TEAS measurements, a new custom-built multicapillary effusive source³⁰ is used. This kind of source has been chosen as it is very compact and reliable. Furthermore, unlike a supersonic source, this type of source needs very little pumping and thus produces very little vibrations or noise, a considerable advantage when used in combination with STM. The He source is mounted at an angle of 45° with respect to the sample surface. A scheme of the source is shown in Fig. 2.

First, ultrapure He gas is used to generate a pressure of ≈ 0.8 mbar in the central tube of the source. The gas then passes through a microchannel plate, a grid of several thousand parallel tubes of a diameter of 10 μm and a length of 0.5 mm. The large aspect ratio leads to a very effective alignment of the gas molecules.³¹ After the channel plate, the He molecules enter an intermediate chamber, which is pumped differentially by a 60 l/s turbomolecular pump. A tube of 0.5 mm in diameter and of 20 mm in length is located 80 mm from the channel plate in the axis of the beam. The gas molecules that are aligned well enough to pass this tube enter the main chamber and form the probing beam. The molecules that do not pass the tube are evacuated via the differential pumping of the intermediate chamber. For our measurements, all information is obtained from the analysis of the intensity change of the specular beam, when clusters or adatoms are deposited on the surface or when moving atoms lead to a structural change on the surface.³² A profile of the resulting beam as measured on the sample, situated 100 mm from the end of the He source is shown in Fig. 3. The velocities of the He atoms in the resulting beam show a Maxwellian thermal distribution, which of course is much larger than the velocity distribution obtained in a supersonic beam. For the planned measurements, the low monochromaticity of the beam is advantageous, as unwanted interference effects are suppressed.

2. He detector

The He detector, mounted in the direction of the specularly reflected beam, is schematically represented in Fig. 4. The detection is achieved in three steps. First, the atoms that

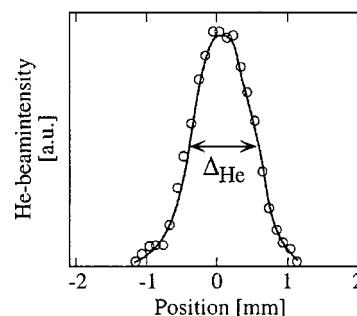


FIG. 3. Profile of the He beam as measured 100 mm from the front end of the He source. FWHM $\Delta_{\text{He}} = 1.1$ mm.

enter the detector are ionized by electron bombardment from a filament. The ionizer part of the detector is surrounded by a cooled Cu cage. Two holes on the axis of the detector allow the He atoms to enter and to leave the cage. The holes also serve to pump the cage. By choosing the appropriate diameter for the two holes and by minimizing the volume of the cage, a high helium partial pressure inside the cage is obtained and the sensitivity of the detector is improved. The ions then pass a series of electrostatic lenses, which align them before they pass into the Wien filter where they are mass separated. Finally, the passing He ions are detected by a channeltron. The Wien filter has been chosen as a mass separator because of its good transmission for incoming atoms, for its simplicity, and small dimensions. The limited mass separation of this type of filter is sufficient to separate the signals coming from the He from those coming from H_2 and H_2O , the next other main peaks in the mass spectra under the experimental conditions. The stability of the signal under typical measuring conditions is $< 2\%$ with a resolution in time < 1 s. A mass resolution $\Delta M/M$ for He of 5 is obtained. As an example, Fig. 5 shows the measured signal/background ratio for our combination of He source and He detector as a function of the sample temperature for a clean Pt(111) surface. The curve shows a Debye–Waller behavior, with an increase of the ratio from 1.6 at 800 K to a maximum of about 13 at a temperature of 100 K.

3. Cluster source

The cluster source has been described in detail elsewhere.³³ It is a CORDIS-type sputtering source, which provides a continuous flux of monodispersed clusters. The

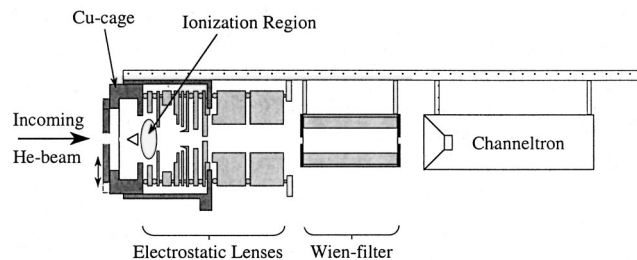


FIG. 4. Layout of the He detector, with the three main parts, ionizer, Wien filter for mass selection, and channeltron for the He detection. The front hole of the Cu cage surrounding the ionizer can be shifted in the horizontal direction. This is necessary, as the manipulator does not have the possibility to tilt the sample to deflect the beam into the manipulator.

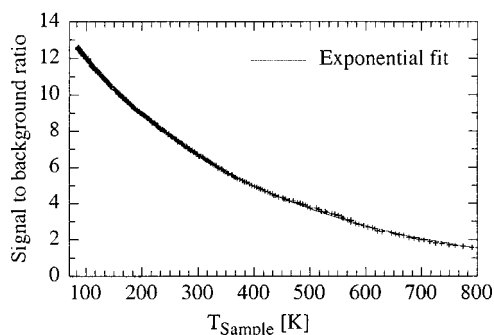


FIG. 5. Measured signal-to-background ratio for our TEAS system: The specular He intensity reflected on a clean Pt(111) surface as a function of the sample temperature T_{sample} shows the exponential Debye–Waller behavior.

clusters are produced by sputtering of the target material with 20 keV rare-gas ions. Cations are extracted with an electrostatic lens and focalized into a Bessel box, which serves as an energy filter. It stops the neutral component of the beam and filters the cations with an energy window of ± 7.5 eV. The mass separation is done by a long quadrupole that follows the Bessel box. The mass resolution is electronically controlled and is adapted to the cluster size under investigation. A mass spectrum for Ag_n^+ clusters obtained from the source is shown in Fig. 6. We typically obtain currents of 0.8–1.3 nA for the silver heptamer. The quadrupole also serves as a guide for the clusters of the selected mass. The incident clusters arrive with an angle of approximately 15° with respect to the surface normal. During deposition, the front end of the quadrupole is placed ≈ 5 –8 mm from the sample surface. The resulting distribution of deposited clusters on the surface has approximately the shape of a Gaussian distribution. Its full width at half maximum (FWHM) depends on the distance of the quadrupole from the surface and on the deposition energy of the clusters. The distance of the quadrupole to the surface is chosen in order to obtain a FWHM which is large (3–4 mm) compared to the one of the probing He beam.

4. Low-temperature manipulator

The custom-built manipulator of the TEAS chamber allows us to perform most of the manipulations necessary for the experiments. It holds the sample during preparation and

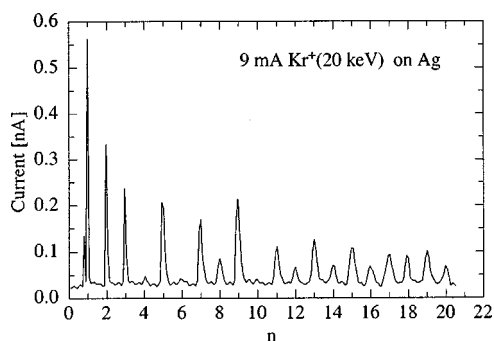


FIG. 6. Typical mass spectra for Ag_n^+ clusters for a primary Kr^+ -ion current of 9 nA on the Ag target and a beam energy of 20 keV. Notice the odd–even alternation and the magic numbers ($n=9$) related to the electronic shell structure.

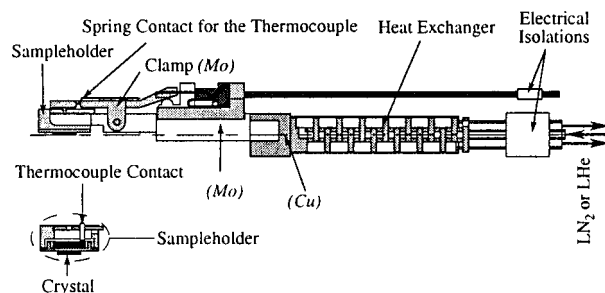


FIG. 7. Details of the head of the manipulator and the sample holder. The Mo clamp, soldered to the front end of the heat exchanger, is operated by a rotary feedthrough.

for the TEAS measurements and it allows transferring the crystal together with the sample holder to the STM chamber. The sample surface can be moved in x , y , and z directions and rotated around the manipulator axis. All displacements are motorized and computer controlled. A long rigid tube supports the functional part of the manipulator, the manipulator head. The manipulator head is shown in Fig. 7.

To obtain the cryogenic temperatures necessary for the experiments, the manipulator is designed as a coaxial liquid-flow cryostat using liquid nitrogen (LN_2) or LHe. The sample holder that contains the sample crystal is held by a clamp system made of molybdenum. The clamp is soldered directly to the heat exchanger and the good thermal conductivity of the molybdenum in the entire used temperature range guarantees an effective cooling of the sample.

The manipulator head is electrically isolated allowing us to apply a potential to the sample. The sample holder, made of two molybdenum pieces, is deposited with the sample inside the STM. A chromel–alumel thermocouple is spot welded directly to the sample crystal. Springs made of the thermocouple material, which are placed on the manipulator head, establish the contact to the thermocouple on the sample holder via two contacts on the back of the sample holder. This system guarantees an accurate determination of the sample temperature in a range between 60 and 1300 K. In contrast, the thermocouple characteristics do not allow us to measure lower temperatures. However, measurements using a Si diode showed that the sample holder reaches a minimum temperature of 20 K when cooled with LHe.

A filament placed directly behind the sample allows the heating of the sample by thermal radiation or electron bombardment in the case where a positive potential is applied to the sample. This permits very fast sample heating with a heating rate up to 50 K/s.

Apart from this equipment, the TEAS chamber also contains an UHV evaporator (type EFM 3 from Omikron³⁴) for the deposition of atoms with thermal energy and an ion gun (type IQE 12/38 from Leybold³⁵) to sputter the sample.

C. Low-temperature STM

The STM chamber containing the microscope and its cooling system is schematically shown in Fig. 8.

1. Cooling system

The cooling system consists of two concentric bath cryostats. The inner cryostat (1), called the LHe cryostat in the

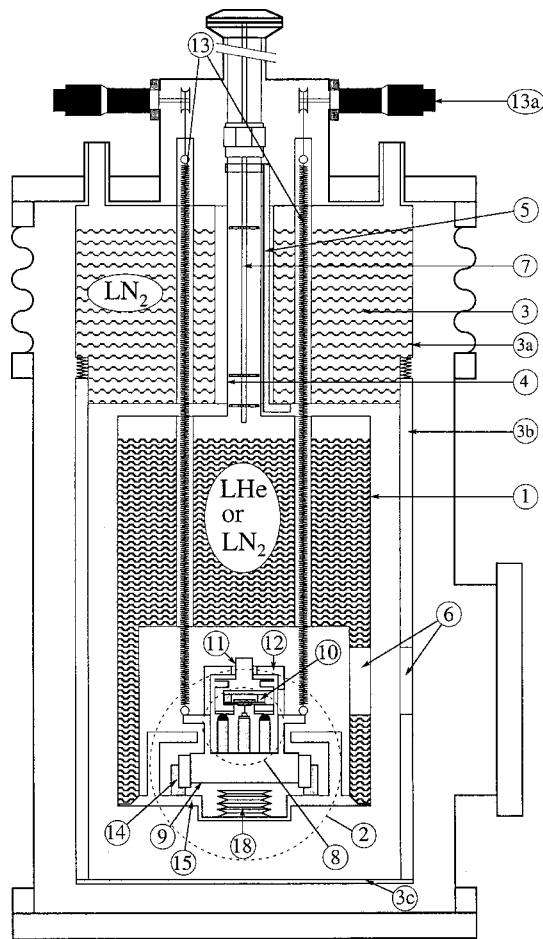


FIG. 8. Layout of the LT-STM. The whole unit, including the two cryostats [(1) and (3)] and the STM (2), is suspended from the top flange of the STM chamber. During STM measurements, the massive STM block (9) containing the scan head (8) and the sample (10) hang freely on long springs (13) from the top flange, guaranteeing a good isolation from vibrations from the STM chamber or the cryostats.

following, contains the STM (2) in a chamber in its lower part. The LHe cryostat can be filled either with LN_2 for measurements down to temperatures of ≈ 78 K or with liquid helium for measurements down to ≈ 8 K. The volume of the cryostat is 3.6 l.

The outer cryostat (3), called the LN_2 cryostat in the following, screens the LHe cryostat against thermal radiation from the environment. It consists of a tank (3a) that contains the liquid nitrogen (5.2 l) and an aluminum cylinder (3b), fixed to the lower part of the tank. Three stainless-steel tubes suspend the tank from the top flange of the chamber. The bottom of the aluminum cylinder is closed with an aluminum cover (3c). The Al cylinder has massive, 7-mm-thick walls to guarantee a good conduction of the heat from the bottom of the tube to its top to minimize the temperature gradient between the top and the bottom.

In order to reduce the LHe consumption and to increase the measuring time, special care has been taken to reduce the thermal losses of the LHe cryostat due to heat conduction and thermal radiation. For this reason, the LHe cryostat and most parts of the STM are gold plated to reduce the emissivity of their surfaces. The LN_2 cryostat is silver plated for the same reason. To reduce losses due to heat conduction, the

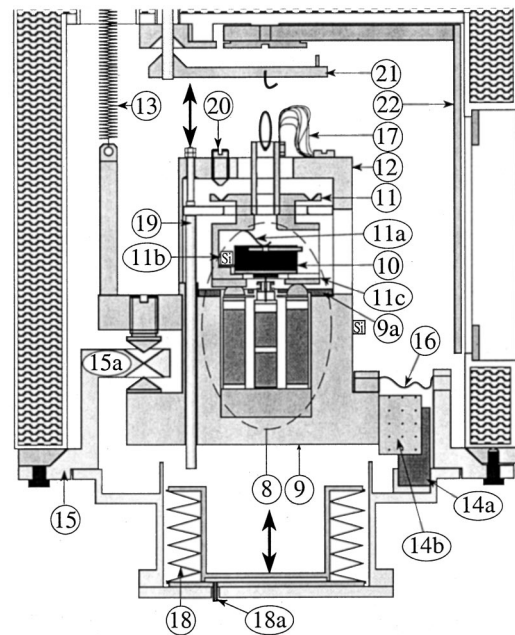


FIG. 9. Detailed view of the STM and the lower part of the LHe cryostat. 80 gold wires (16) connecting the STM block (9) to the support ring (15) that is directly screwed to the LHe cryostat provide cooling of the microscope during measurements. The whole measuring unit, including the STM block and the support ring, can be removed in a simple way for maintenance.

suspension tube (4) of the LHe cryostat has been chosen long and with thin walls. A solid Cu rod (5) establishes a thermal bridge from the bottom of the LN_2 cryostat to the top of the support tube and cools the tube to ≈ 80 K at this point. Likewise, all other connections to the LHe cryostat are precooled by anchoring them thermally to the LN_2 cryostat.

Both cryostats have an opening (6) in the direction of the TEAS chamber to allow the sample transfer. These openings are closed by metal doors during the STM measurements to block heat radiation on the STM. Large view ports in both cryostats allow visual control of all manipulations of the STM. The view port of the inner cryostat is screened with a sapphire window, while for the outer cryostat a combination of a sapphire and a Pyrex window is used to screen the microscope against thermal radiation. This combination transmits light in a wavelength range between 0.3 and 3 μm , screening the inner cryostat against infrared radiation from the environment at 300 K. To ensure a good thermal contact a thin indium seal is pressed between the windows and cryostat.

When the LHe cryostat contains liquid helium, a thin stainless-steel tube with Cu screening disks (7) is introduced into the suspension tube.

2. Microscope

The scan head of the microscope (8) is a custom-built, modified "Beetle-style" scan head.³⁶ The piezos (type EBL2 from Staveley Sensors Inc.³⁷) have a diameter of 6.35 mm and a length of 24.6 mm. A 0.2-mm-thick tantalum triangle (see Fig. 9) connects the top of the three coarse approach piezos solidly, improving the stiffness of the unity and increasing its resonance frequency.

The whole piezounit is surrounded by the massive copper block (9) called the STM block in the following. A gold-plated copper disk (9a) is screening the piezos against heat radiation from the drawer (11), in case the latter is heated.

On transfer into the STM chamber, the sample holder (10) is pushed into the drawer. A good thermal contact between drawer and sample holder is assured by a spring (11a). The drawer contains a Si diode (11b) (type DT470-SD from Lake Shore Cryogenics Inc.³⁸). It is placed as close as possible to the sample holder to allow an accurate determination of the sample temperature. A massive Cu piece (12) that surrounds the drawer is screwed to the top of the STM block. The Al disk with the ramp (11c) for the coarse approach between sample and tip is screwed to the bottom of the drawer. The drawer stands on the coarse approach piezos. To simplify the construction and to avoid unnecessary heat conduction to the LHe cryostat through cables with a large cross section, no resistive sample heating has been installed in the drawer. The heating of the sample is achieved by focalizing the beam of an Ar laser on the sample holder or the drawer. A small part of the drawer is covered with a carbon film. This spot with improved radiation absorption ($\epsilon=1$) serves as a target for the laser. As a Si diode is placed in the drawer the maximal temperature permitted is 450 K. The performances of the heating system will be discussed in Sec. II C 4.

During measurements, the STM block is suspended freely from the top flange of the STM chamber on three 60-cm-long springs (13), which pass the two cryostats inside tubes. The choice of long springs and the heavy mass of the STM block (1.3 kg) lead to a low eigenfrequency of 0.8 Hz for vertical oscillations of the block. This arrangement isolates the STM effectively against vibrations from the chamber or from the cryostats. The springs are suspended on Kantal wires. These can be enrolled on the axis of three rotary feedthroughs (13a) allowing us to adjust the length of the springs. This is necessary, as the springs get much stiffer and consequently reduce their length when cooled down to cryogenic temperatures (by ≈ 2 cm when cooled from 300 to 77 K). An eddy-current damping system (14) is installed around the bottom part of the block, serving as a damping element for the oscillations of the block. It consists of 12 CoSm magnets (14a) fixed on the STM support ring and copper flaps (14b) fixed on the STM block. As the damping forces are proportional to $1/\rho$ [where $\rho(T)$ is the electrical resistance of the flaps], the damping gets much stiffer when the STM is working at low temperatures where ρ is low.³⁹ We have chosen the geometry of our flaps in order to allow a sufficiently weak damping at LHe temperature and we used unannealed Cu to reduce the differences between the resistance at high and low temperature.

The STM block is surrounded by a support ring (15). The ring has three radial arms (15a) separated by 120° , with conic holes on the top and the bottom. Two cones, fixed on the block, enter the conic holes on the arm from above and underneath. This limits the vertical and the horizontal movements of the block to the distance between the cones.

The cooling of the STM is done in two different modes; During the STM measurements, the thermal contact between the STM block and the LHe cryostat is guaranteed by ≈ 80

gold wires (16) of a diameter of 0.2 mm. These connect the block radially to the massive Cu support ring that is directly screwed to the bottom of the LHe cryostat. The very soft material of the wires translates very little vibrations from the cryostat to the block. Likewise, the contact between the STM block and the drawer is established by 20 Cu wires (17) of the same diameter. These are electrically isolated to allow us to apply a bias potential to the drawer. This cooling mode is sufficient to compensate the thermal radiation on the drawer and to keep the sample at low temperature during measurements.

When a more effective cooling is needed to cool down the STM from higher temperatures, the STM block can be pressed against the arms (15a) of the ring by means of a manipulator bellow (18), which is placed underneath the block. The bellow can be filled and pumped via a microtube (18a). He gas is used to fill the bellow to avoid condensation inside the tube at low temperatures. The block is pressed up by the bellow with a maximal force of 100 N and under this condition a very good thermal contact is guaranteed. When pressed up, the lower cones of the STM block enter the lower cones of the arms of the ring. In this way, the position of the block is fixed exactly, which is essential for the sample transfer to or from the TEAS chamber. The bellow, by means of a piston system (19), also presses the drawer up against the piece (12) that surrounds it. This way, a good thermal contact to the drawer and the sample is established. Three cones (20) fix the orientation of the drawer during the sample transfer.

The bellow also allows us to lift up the drawer from the piezos very precisely. By regulating the pressure in the bellow the drawer can be lifted or lowered with a precision of ≈ 0.1 mm.

A manipulator in the STM chamber (21) is used to lift up and move the drawer and to open and close the rotary door (22) of the LHe cryostat.

3. Performance of the cooling system

A filling of the LHe cryostat lasts for up to 28 h while the LN₂ cryostat has to be refilled every 14 h. The time between two successive tank fillings is long enough to allow comfortable handling of the STM.

The cooling behavior of the LN₂ cryostat, the STM block, and the sample, when cooled down from room temperature, are shown in Fig. 10. The temperature on the outer cryostat is measured by means of a chromel–alumel thermocouple on the outer surface of the screening tube, 2 cm above its lower end. A second Si diode of the same type as the one measuring the sample temperature is used to measure the temperature of the STM block.

With drawer, STM block, and support ring pressed together by the manipulator bellow, a temperature of 80 K of the sample and the STM block is reached within 90 min after the inner cryostat has been filled with LN₂. Then, the cooling slows down and the temperatures stabilize on their minimum values within 3 h. After this, the STM block is released in its free-hanging measuring position with a minimum sample temperature of 78.5 K.

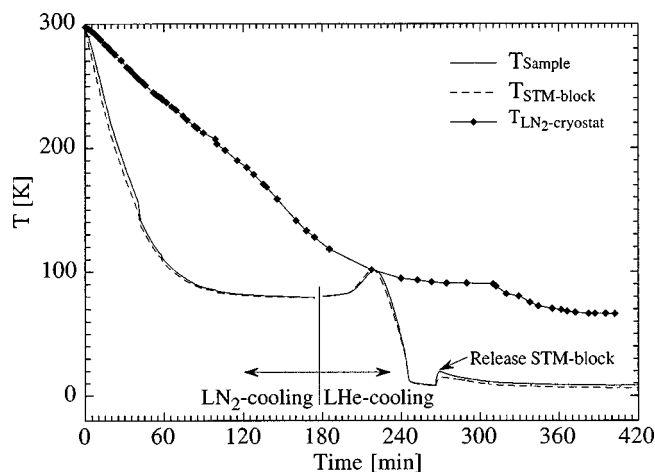


FIG. 10. Temperature behavior of the LN₂ cryostat, the STM block, and the sample when cooled down from room temperature to the lowest possible temperatures. The increase when the block is released in its free-hanging position is due to the thermal radiation of the light used to survey the manipulations.

For measurements at lower temperature, the LN₂ in the inner cryostat is replaced by LHe. A temperature of 10 K is reached within 40 min after the start of the filling with LHe. Then, the STM block is released in its free-hanging position by reducing the pressure in the manipulator bellow and the sample temperature stabilizes at its minimum value of 7.9 K within 150 min, with the STM block at 5.7 K. Approximately 15 l of liquid helium are needed to cool down the inner cryostat and the STM from LN₂ to LHe temperature.

The temperature measured at the lower end of the LN₂ cryostat decreases much slower as the whole massive aluminum screening tube has to be cooled down. A final temperature of 90 K is reached after ≈ 5 h. During the STM measurements the LN₂ cryostat is pumped to solidify the liquid nitrogen to avoid bubbling, causing unwanted vibrations which would disturb the measurement. The solidification of the LN₂ leads to a further decrease of the temperature measured on the LN₂ cryostat to ≈ 66 K.

4. Sample heating by laser

To heat the sample, the beam of an Ar laser with an output power of 5–6 W is focalized on the sample or the drawer. Approximately 40% of the laser output power is used to heat the sample, while the rest is absorbed and reflected by the screening windows and the different optical elements employed (two mirrors and one focalizing lens).

Two different heating modes are used, depending on whether the inner cryostat is cooled with LN₂ or with LHe.

In the first case, the sample can be heated up to a given temperature and be stabilized at this temperature. The temperature of the sample can be stabilized on every intermediate temperature between 77 and 450 K by regulating the output power of the laser with a feedback loop on the temperature measurement. The stability of the temperature is $< \pm 0.01$ K. Up to 300 K, the stability of the STM is good and only a small amount of drift is observed, allowing occasionally atomic resolution on Pt(111). At temperatures higher than 300 K the continuous irradiation of the sample

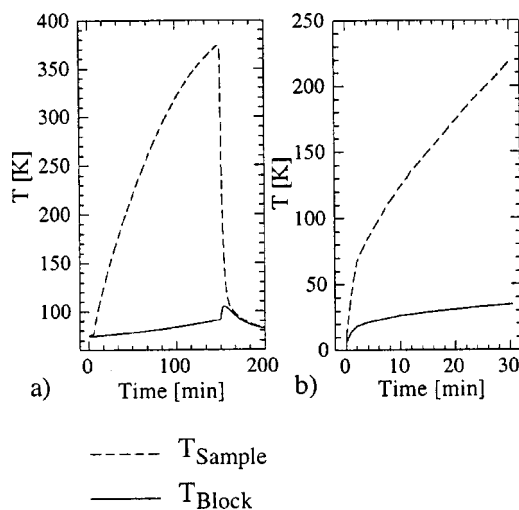


FIG. 11. Temperature behavior of the sample and the STM block when heated with the laser: (a) When using LN₂ as a cooling liquid (laser output power 5.2 W) after the heating, drawer, STM block, and support ring are pressed together by the manipulator bellow and the sample is rapidly cooled down again. (b) When using LHe as a cooling liquid (laser output power 5.7 W).

holder with more than one watt leads also to a temperature increase of the STM block and the piezos, resulting in a stronger drift.

When LHe is used as a cooling liquid, continuous heating would lead to a high LHe consumption. Therefore, in this case, we only heat the sample until the desired maximum temperature is reached, then stop the laser and cool back down the sample to the lowest possible temperature. This procedure also allows us to make use of the good stability of the STM at low temperature, which allows us to obtain atomic resolution on Pt(111) regularly. The temperature behavior of the sample and the STM block when heated with the laser is shown in Fig. 11 for the two cryogenic liquids for output powers of 5.2 and 5.7 W, respectively. In the case of LN₂ the sample reaches 200 K within 37 min, while heating up to 373 K takes about 2 h 25 min. To cool down the sample and the block rapidly, they are pressed against each other and against the support ring.

With LHe as a cooling liquid, the temperature first increases very quickly, as the heat capacity of the drawer and sample holder is very small at low temperature, and a temperature of 70 K is reached within 2 min. It takes ≈ 30 min to reach a sample temperature of 220 K.

In both cases the temperature increase of the STM block due to the thermal radiation from the hot drawer and the conduction in the wires for the cooling is small compared to the temperature of the sample.

5. Resonances of the STM

Mechanical vibrations from the environment are very effectively damped by the two-stage damping system (First stage: heavy table on vibration isolation feet; second stage: suspension springs of the STM block). Isolation against acoustic noise is made by the sound isolating box, surrounding the STM chamber. To avoid that eigenmodes of the STM are excited by the remaining external vibrations or vibrations

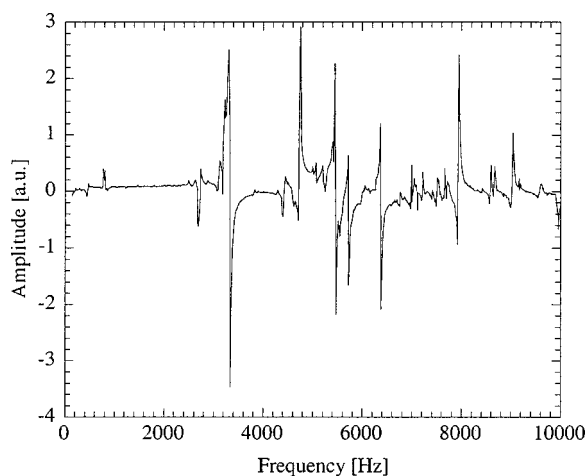


FIG. 12. Resonance spectrum of the STM. We have simulated an external vibration by applying a sinusoidal tension (2 V pp) to the x^+ electrode of the scan piezo, while we were monitoring the in-phase piezoelectric voltage pick-up on the x^+ electrode of a coarse approach piezo (see Ref. 40).

induced by the scanning movement of the piezo, we have chosen a very rigid design of the piezounit. This has been achieved by using rigid piezotubes with a large diameter and by further rigidifying the unit by connecting the top ends of the coarse approach piezo with a tantalum triangle. Furthermore, unlike in many other STM designs, the piezos are mounted on a heavy mass (STM block), which is ineffectively excited by the piezo movement. The resonance spectrum of the STM, measured at LHe temperature, is shown in

Fig. 12.⁴⁰ Besides a resonance at 945 Hz, the first major resonances are found at frequencies of 2800 and 3200 Hz. External vibrations of these high frequencies are well damped by the damping system and they lay well above the scanning frequency.

III. EXPERIMENTAL RESULTS

We present the first high-resolution STM images obtained after deposition of metal clusters on a metal surface as well as in a Xe matrix.

The Pt(111) sample has been prepared by means of Ar-ion sputtering (several hours with 1000 eV at $T_{\text{sample}}=400$ K), annealing up to 1050 K, and exposure to an O_2 partial pressure of 1×10^{-7} for 3 min at $T_{\text{sample}}=900-1000$ K. The cleanliness of the surface and the cluster deposition have been monitored by TEAS.

A. Deposition of Ag_7^+ on Pt(111) with $E_{\text{kin}}=95$ eV at $T_{\text{sample}}=93$ K

After the deposition of the clusters, a large number of spots with a diameter of ≈ 15 Å are observed on the surface, which we identify as the cluster impacts. At higher magnification, the atomic structure of some of these impacts could be resolved. A typical example is shown in Fig. 13. The impact region can be divided in three parts; zone 1 is most probably the central impact zone, characterized by a certain disorder of the atoms. They are not in registry with the atoms of the surface or the adsorption sites on the surface and im-

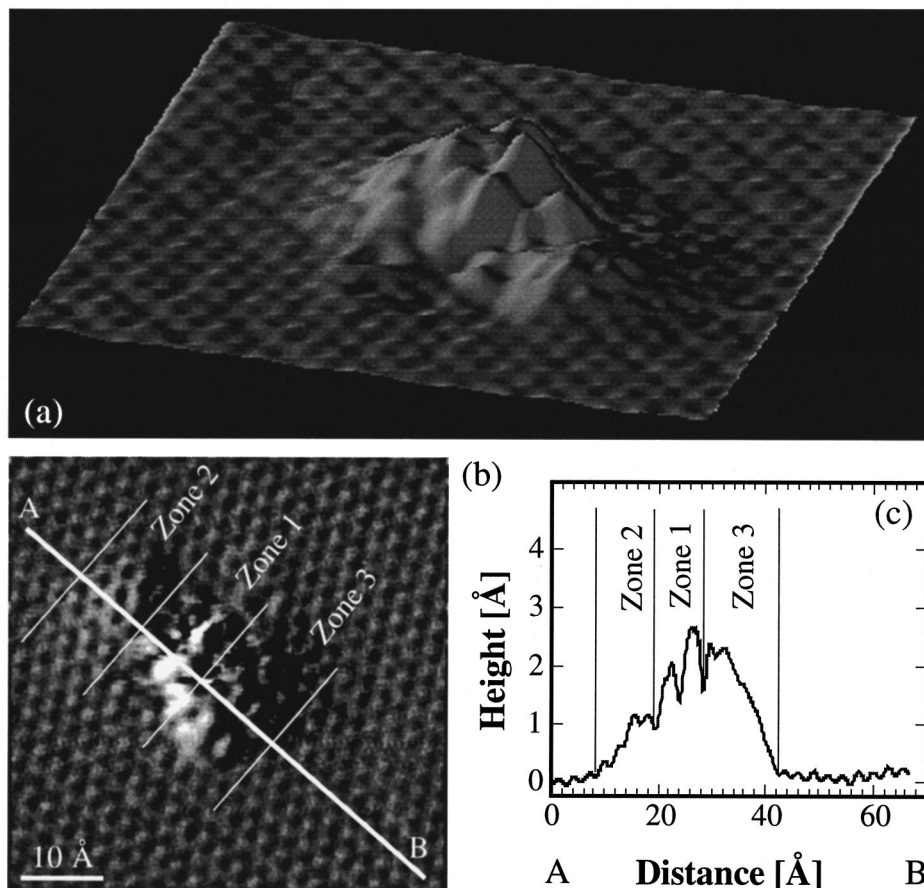


FIG. 13. The cluster impact zone after deposition of Ag_7^+ with 95 eV at $T_{\text{sample}}=93$ K, $T_{\text{measure}}=8.4$ K. (a) Three-dimensional projection of the STM image, (b) top view of the same zone ($53 \text{ Å} \times 53 \text{ Å}$), dz/dx mode to get contrast on cluster and surface, and (c) line scan as marked in (b).

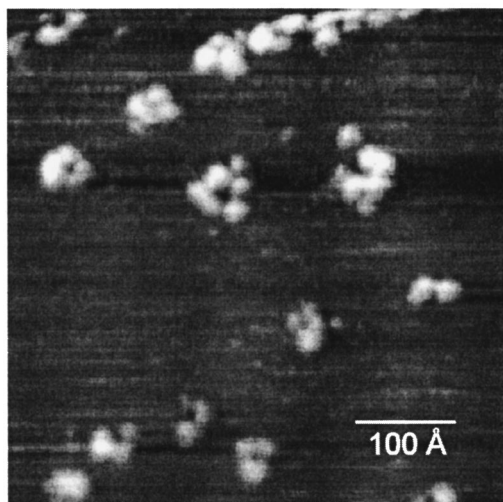


FIG. 14. STM image of the surface after deposition of Ag_7^+ clusters with 1000 eV at $T_{\text{sample}}=93$ K ($500 \text{ \AA} \times 500 \text{ \AA}$, $T_{\text{measure}}=62$ K).

aged at random height. In zones 2 and 3 the lateral positions of the atoms correspond to the one of the Pt lattice. These atoms are imaged gradually higher than the surface as one approaches zone 1 (see the line scan).

The apparent disorder in zone 1 could be an indication that local melting has taken place in the impact region and that the material has been quenched in an amorphous state in the subsequent ultrafast cooling. The image of melting at the impact is in agreement with the results of several MD simulations for clusters with impact energies of 3.5–30 eV per atom.^{1,2,6} Kaiser, Bernhardt, and Rademan explain their STM images of Sb_8^+ clusters deposited on highly oriented pyrolytic graphite with 26 eV per atom with local melting.¹⁹

B. Deposition of Ag_7^+ on Pt(111) with $E_{\text{kin}}=1000$ eV at $T_{\text{sample}}=93$ K

When the impact energy of the clusters is increased to 1000 eV, the situation changes completely (Fig. 14). The impacts consist of a central impact region, a vacancy island (crater) with a diameter of 10–15 Å, and small approximately round islands of substrate atoms ejected onto the surface decorating the rim of the crater. The measured diameter of the impact zone (crater+islands) is 40 ± 10 Å. Typically, 3–4 islands are found around a vacancy island. Sometimes craters with just one or with up to seven islands are observed.

Analysis of the images show that per impact an average of 80 ± 20 atoms have been ejected onto the surface. On the other hand, the size of the craters corresponds to only 25 vacancies. Even when taking into account tip effects and the seven additional atoms from the cluster, the number of adatoms on the surface is superior to the expected value.

We conclude that these additional adatoms are ejected from inside the bulk and that a great number of bulk vacancies have been produced by the cluster impacts. This effect has also been observed by STM for rare-gas sputtering with energies in the kV range on Pt(111) by Michely and Teichert.⁴¹

The two experiments presented here clearly demonstrate the possibilities of our STM as a tool to investigate the

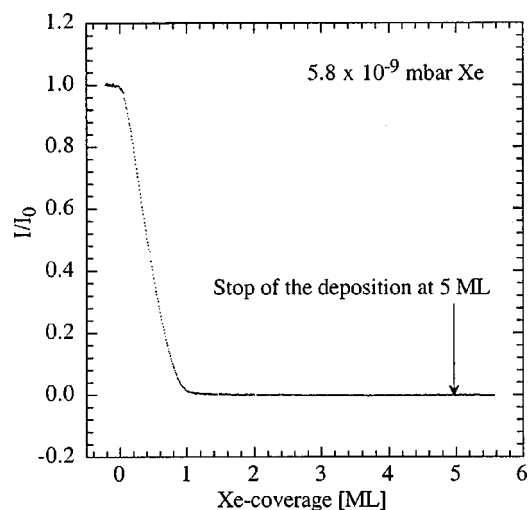


FIG. 15. Normalized intensity I/I_0 of the specularly reflected He beam during the deposition of Xe–rare-gas layers on Pt(111) at $T_{\text{sample}} \approx 30$ K.

cluster-surface-collision outcome on a microscopic scale. The above interpretations must, however, be considered as preliminary and the few experiments performed do not allow us to draw definite conclusions yet. More experiments at a lower deposition temperature are needed, since at a surface temperature of 93 K where these experiments were performed, Ag and Pt adatoms are highly mobile and can diffuse away from the impact zone.

Systematic studies of the collision outcome in the range from the lowest possible energy (soft landing) up to the keV energy range are now underway, combining STM and TEAS to take advantage of the full potential of the new setup.

C. Deposition of Ag_7^+ in 5+2 ML of Xe on Pt(111) with $E_{\text{kin}}=20$ eV at $T_{\text{sample}}=20$ K

As we plan to do a number of STM and STS measurements with soft-landed clusters or clusters that are still partially embedded in the rare-gas matrix, we have deposited Ag_7^+ clusters on a Xe matrix to get a first impression of what has to be expected.

For the deposition of the rare-gas layer, a partial pressure of 5.8×10^{-9} mbar of Xe was introduced into the TEAS chamber with the sample at ≈ 30 K. The deposition was monitored by TEAS. This allowed us to determine the total coverage within a few percent of a monolayer. The measured TEAS signal for the Xe deposition is shown in Fig. 15. A total of 5 ML were deposited. Figure 16 shows the Pt(111) surface with a multilayer coverage of Xe. The Xe adlayer orders in a higher-order commensurate phase.⁴² This leads to a buckling with a period of 24.1 ± 0.7 Å that has been observed earlier by STM for a 1 ML covering.⁴³ Our measurements nicely confirm the rotation of the adlayers and show that the buckling is also present at a coverage of several monolayers.

The deposition of the 5 ML of Xe was followed by the deposition of Ag_7^+ clusters, with an incident energy of 20 eV. 2 ML of Xe were added after the end of the cluster deposition to cover the clusters and parts of the surface that may have been uncovered during the cluster deposition. This ad-

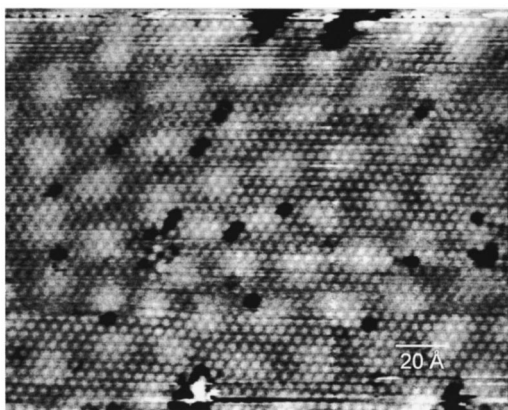


FIG. 16. Atomically resolved STM image of the buckled multilayer Xe matrix adsorbed on Pt(111) ($200 \text{ \AA} \times 160 \text{ \AA}$, $T_{\text{measure}} = 8 \text{ K}$).

ditional coverage should protect the clusters and the surface from any contamination. An image obtained after this deposition is shown in Fig. 17. We observe large terraces, covered with the rare gas, which are strewn with a large number of small hillocks, all having approximately the same diameter of 20 \AA . We conclude that these protrusions on the rare-gas matrix mark the points where a cluster is buried inside the matrix. The matrix atoms on top of the clusters are imaged by, at most, 1.4 \AA higher than the surrounding matrix atoms. Some of the atoms on the hillock have moved laterally by some tenths of an angstrom from their position on the undisturbed Xe lattice.

The fact that it is possible to identify the position of a cluster, even if it is buried inside several layers of rare gas, shows that it is possible to investigate clusters by STM or STS while they are still in the matrix. Further experiments will have to show if one can obtain uncovered clusters and if in this case the interaction between the cluster and the matrix is strong enough to prevent the cluster to be moved by the tip.

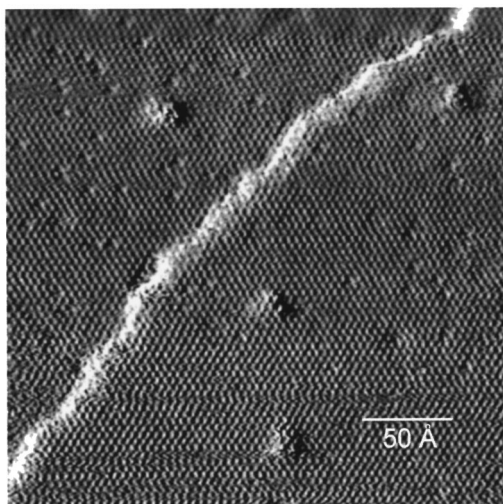


FIG. 17. Atomically resolved STM image of the Xe matrix after the deposition of Ag_7^+ clusters with 20 eV incident kinetic energy on 5 ML of Xe followed by the deposition of 2 ML of Xe. The four hillocks are identified as the position of the buried clusters ($300 \text{ \AA} \times 300 \text{ \AA}$, dz/dx mode, $T_{\text{measure}} = 8 \text{ K}$).

IV. DISCUSSION

We have presented a new experimental setup combining TEAS and STM as experimental techniques for the investigation of the processes occurring when clusters are deposited on a well-defined surface. The setup is separated into two chambers, one containing the STM, the other the rest of the experimental equipment. A transfer chamber connects the two chambers for sample transfer, while during STM measurements the two chambers are mechanically separated in order to isolate the microscope from vibrations.

This modular layout is highly versatile and guarantees UHV conditions and cryogenic temperatures at all times including the sample transfer.

A new compact multichannel effusive He source in combination with a new Wien-filter-based He detector are used for the TEAS measurements. A custom-built manipulator allows us to transfer the sample between the two chambers and to perform most manipulations necessary for the experiment. It includes a liquid-flow cryostat as well as a sample heating and allows sample temperatures in the range of $\approx 30\text{--}1300 \text{ K}$.

The new low-temperature STM is based on a ‘‘Beetle-style’’ scan head. A two-stage damping system is used to isolate the microscope effectively from mechanical vibrations. The STM is placed inside a LHe cryostat that cools down the whole microscope and ensures stable measuring conditions with a low drift rate and a minimum sample temperature of 8 K . A laser beam focalized on the sample holder is used to heat the sample. This system allows us to stabilize the sample temperature on any intermediate value between 8 K and the maximal temperature of 450 K with an accuracy of $< \pm 0.01 \text{ K}$.

The performances of the STM are illustrated with high-resolution images obtained after the deposition of Ag_7^+ clusters with impact energies of 95 and 1000 eV at $T_{\text{sample}} = 93 \text{ K}$ showing a very different collision outcome in the two cases.

First images of Ag_7^+ clusters deposited with $E_{\text{kin}} = 20 \text{ eV}$ in a 7-ML -thick Xe matrix adsorbed on Pt(111) show that it is possible to identify the position of these soft-landed clusters even when embedded inside the matrix.

ACKNOWLEDGMENTS

This work was supported by the Swiss National Fund and by the I.C.S. World Laboratory for one of the authors (A.B.).

¹H. Hsieh, R. S. Averback, H. Sellers, and C. P. Flynn, Phys. Rev. B **45**, 4417 (1992).

²H. P. Cheng and U. Landman, J. Phys. Chem. **98**, 3572 (1994).

³R. S. Averback and M. Galy, Nucl. Instrum. Methods Phys. Res. B **90**, 191 (1994).

⁴P. Blandin and C. Massobrio, Surf. Sci. Lett. **279**, L219 (1992).

⁵G. Vandoni, Ch. Félix, and C. Massobrio, Phys. Rev. B **54**, 1553 (1996).

⁶G. Betz and W. Husinsky, Nucl. Instrum. Methods Phys. Res. B **122**, 311 (1997).

⁷G. Vandoni, Ch. Félix, C. Goyhenex, R. Monot, J. Buttet, and W. Harbich, Surf. Sci. **331-333**, 838 (1995).

⁸G. Vandoni, Ch. Félix, R. Monot, J. Buttet, C. Massobrio, and W. Harbich, Surf. Rev. Lett. **3**, 949 (1996).

⁹Ch. Félix, G. Vandoni, C. Massobrio, R. Monot, J. Buttet, and W. Harbich, Phys. Rev. B **54**, 1553 (1996).

- ¹⁰T. M. Bernhardt, B. Kaiser, and K. Rademan, *Z. Phys. D: At., Mol. Clusters* **40**, 327 (1997).
- ¹¹R. D. Beck, J. Rockenberger, P. Weiss, and M. M. Kappes, *J. Chem. Phys.* **104**, 3638 (1996).
- ¹²A. Terasaki, T. Tsukuda, H. Yasumatsu, T. Sugai, and T. Kondow, *J. Chem. Phys.* **104**, 1387 (1996).
- ¹³H. Yasumatsu, A. Terasaki, and T. Kondow, *J. Chem. Phys.* **106**, 3806 (1997).
- ¹⁴H. V. Roy, P. Fayet, F. Patthey, W. D. Schneider, B. Delley, and C. Massobrio, *Phys. Rev. B* **49**, 5611 (1994).
- ¹⁵S. B. DiCenzo, S. D. Berry, and E. Hartford, Jr., *Phys. Rev. B* **38**, 8465 (1988).
- ¹⁶W. Eberhardt, P. Fayet, D. M. Cox, Z. Fu, A. Kaldor, R. Sherwood, and D. Sondericker, *Phys. Rev. Lett.* **64**, 780 (1990).
- ¹⁷U. Heiz, F. Vanolli, A. Sanchez, and W. D. Schneider, *J. Am. Chem. Soc.* **120**, 9668 (1998).
- ¹⁸D. Lovall, M. Buss, R. P. Andres, and R. Reifenberger, *Phys. Rev. B* **58**, 15889 (1998).
- ¹⁹B. Kaiser, T. M. Bernhardt, and K. Rademan, *Appl. Phys. A: Mater. Sci. Process.* **66A**, 711 (1998).
- ²⁰S. J. Carroll, P. Weibel, B. von Issendorff, L. Kuipers, and R. E. Palmer, *J. Phys.: Condens. Matter* **8**, 617 (1996).
- ²¹Y. Kuk, M. F. Jarrold, P. J. Silverman, J. E. Bower, and W. L. Brown, *Phys. Rev. B* **39**, 11168 (1989).
- ²²L. Bardotti, P. Jensen, A. Hoareau, M. Treilleux, and B. Cabaud, *Phys. Rev. Lett.* **74**, 4694 (1995).
- ²³S. J. Carroll, K. Seger, and R. E. Palmer, *Appl. Phys. Lett.* **72**, 305 (1998).
- ²⁴W. Harbich, Y. Belyaev, R. Kleiber, and J. Buttet, *Surf. Rev. Lett.* **3**, 1147 (1996).
- ²⁵S. Fedrigo, W. Harbich, and J. Buttet, *J. Chem. Phys.* **99**, 5712 (1993).
- ²⁶H. P. Cheng and U. Landman, *Science* **260**, 1304 (1993).
- ²⁷M. Ratner, W. Harbich, and S. Fedrigo, *Phys. Rev. B* **60**, 11730 (1999).
- ²⁸K. Bromann, C. Félix, H. Brune, W. Harbich, R. Monot, J. Buttet, and K. Kern, *Science* **274**, 956 (1996).
- ²⁹Newport Corporation, 1791 Deere Avenue, Irvine, CA 92714.
- ³⁰F. Maier, S. Kneitz, H. Koschel, and H.-P. Steinrück, *Surf. Sci.* **377-379**, 1101 (1997).
- ³¹*Atomic and Molecular Beam Methods*, edited by G. Scoles (Oxford University, New York, 1988), Vol. 1.
- ³²A general introduction to the TEAS technique is given in B. Poelsema and G. Comsa, *Scattering of Thermal Energy Atoms from Disordered Surfaces*, Springer Tracts in Modern Physics (Springer, Berlin, 1989), Vol. 115.
- ³³G. Vandoni, Ch. Félix, R. Monot, J. Buttet, and W. Harbich, *Chem. Phys. Lett.* **229**, 51 (1994).
- ³⁴Omikron Vakuumphysik GmbH, Idsteinerstrasse 78, D-65232 Taunusstein.
- ³⁵Leybold-Heraeus GmbH, Bonner Strasse 498; D-50000 Köln.
- ³⁶K. Besocke, *Surf. Sci.* **181**, 145 (1987).
- ³⁷Staveley Sensors, Inc., 91 Prestige Park Circle, East Hartford, CT 06108.
- ³⁸Lake Shore Cryotronics, Inc., 64 East Walnut St., Westerville, OH 43081-2399.
- ³⁹K. Nagaya and H. Kojima, *J. Dyn. Syst., Meas., Control* **106**, 46 (1984).
- ⁴⁰S. Behler, M. K. Rose, D. F. Ogletree, and M. Salmeron, *Rev. Sci. Instrum.* **68**, 124 (1997).
- ⁴¹T. Michely and T. Teichert, *Phys. Rev. B* **50**, 11156 (1994).
- ⁴²K. Kern, R. David, R. L. Palmer, and G. Comsa, *Phys. Rev. Lett.* **56**, 2833 (1986).
- ⁴³S. Horch, P. Zeppenfeld, R. David, and G. Comsa, *Rev. Sci. Instrum.* **65**, 3204 (1994).